CHIN. PHYS. LETT. Vol. 37, No. 8 (2020) 087401 **Express Letter**

Zirconium Aided Epitaxial Growth of In_xSe_y on InP(111) Substrates

Cheng Zheng(郑澄)[1], Dapeng Zhao(赵大鹏)[1,2], Xinqiang Cai(蔡新强)[1], Wantong Huang(黄万通)[1], Fanqi Meng(孟繁琦)[3], Qinghua Zhang(张庆华)[3], Lin Tang(唐林)[1], Xiaopeng Hu(胡小鹏)[1], Lin Gu(谷林)[3], Shuai-Hua Ji(季帅华)[1,4*], Xi Chen(陈曦)[1*]

[1]*State Key Laboratory of Low Dimensional Quantum Physics, Department of Physics, Tsinghua University, Beijing 100084, China*
[2]*Beijing Academy of Quantum Information Sciences, Beijing 100193, China*
[3]*Laboratory for Advanced Materials & Electron Microscopy, Beijing National Laboratory for Condensed Matter Physics, Institute of Physics, Chinese Academy of Sciences, Beijing 100190, China*
[4]*RIKEN Center for Emergent Matter Science (CEMS), Wako 351-0198, Japan*

(Received 20 June 2020; accepted 30 June 2020; published online 02 July 2020)

Layered material indium selenide (In_xSe_y) is a promising candidate for building next-generation electronic and photonic devices. We report a zirconium aided MBE growth of this van der Waals material. When co-depositing zirconium and selenium onto an indium phosphide substrate with a substrate temperature of 400℃ at a constant zirconium flux rate of 0.01 ML/min, the polymorphic In_xSe_y layer emerges on top of the insulating $ZrSe_2$ layer. Different archetypes, such as InSe, α-In_2Se_3 and β-In_2Se_3, are found in the In_xSe_y layers. A negative magnetoresistance of 40% at 2 K under 9 T magnetic field is observed. Such an $In_xSe_y/ZrSe_2$ heterostructure with good lattice-matching may serve as a candidate for device applications.

PACS: 74.70.Xa, 81.15.Hi, 74.78.Fk DOI: 10.1088/0256-307X/37/8/087401

The past two decades have witnessed much progress of pursuing novel materials as building blocks for next-generation electronic and photonic devices.[1–5] Two-dimensional van der Waals (vdW) materials, such as graphene,[6] black phosphorus[7] and various kinds of transition-metal dichalcogenides[8–12] (TMD), all serve as promising candidates because of their appealing electronic, optical, thermal and even mechanical properties. In the family of vdW materials, extensive studies were performed in recent years on the layered-structure Ⅲ–Ⅵ group metal chalcogenides,[13–16] among which indium selenide (In_xSe_y) has stimulated great interest for its novel properties and the potential of fabricating high-performance devices.[17–26] Until now, most progresses were made by using exfoliated samples. Tamalampudi *et al.* reported that the photoresponsivity of broadband few-layer InSe photodetectors could be greatly enhanced from 6.9 to 157 $A\cdot W^{-1}$ by applying 70 V back-gate voltage.[18] Bandurin *et al.* found that the electron density in an atomically thin film of InSe could be controlled by gate voltage in a wide range, and therefore discovered in this thin film a high Hall mobility of $\sim 10^3$ $cm^2\cdot V^{-1}s^{-1}$ at room temperature and $\sim 10^4$ $cm^2\cdot V^{-1}s^{-1}$ at liquid helium temperature.[20] Si *et al.* created a new type of field-effect transistors (FETs) in which α-In_2Se_3, a ferroelectric semiconductor, was employed as the channel material.[26] Such FETs could be useful in future non-volatile memory technology. Generally, it is highly desirable to build heterostructures made of In_xSe_y together with insulating layers for gating.

Layered In_xSe_y single crystals can exist at ambient pressure in several different stoichiometries, such as InSe and In_2Se_3, each having various polymorphs.[27–32] InSe is formed by the stacking of Se–In–In–Se atomic layers. β, γ and ε phases of InSe differ in the stacking sequences from each other. However, the layered α-In_2Se_3 and β-In_2Se_3 are determined by the atomic arrangements inside a single Se–In–Se–In–Se building block, while different stacking sequences are denoted by 2H and 3R.

Despite the success of obtaining exfoliated flakes of In_xSe_y crystals grown by the Bridgman method,[33] the size of such flakes limits its potential for further investigations. Therefore, it is worthwhile to explore the approaches to grow In_xSe_y thin films. The growth of a highly oriented two-dimensional vdW crystal usually relies on a substrate of small lattice mismatch, even though the lacking of dangling bonds makes the vdW materials to be easily grown on various substrates with a sharp interface and low in-plain strain. To date, the attempts to epitaxially grow different phases of In_xSe_y, whether by chemical vapor deposition (CVT), physical vapor transport (PVT) or molecular beam epitaxy (MBE), have been made on var-

Supported by the National Natural Science Foundation of China (Grant No. 11874233).
*Corresponding authors. Email: shji@mail.tsinghua.edu.cn; xc@mail.tsinghua.edu.cn
© 2020 Chinese Physical Society and IOP Publishing Ltd

ious substrates such as graphene,[24,34] GaAs,[35,36] MoS_2,[37] GaSe,[38,39] SiO_2/Si,[25,40–42] mica[23,43,44] and Corning glass,[45] most of which are of large lattice mismatching. For device applications, it is still essential to find insulating substrate materials with good lattice-matching with In_xSe_y to build heterostructures.

In this study, we establish an approach to preparing heterostructure of In_xSe_y and insulating $ZrSe_2$ by MBE on an InP(111) substrate. The flatness of the $ZrSe_2$ layers in large scale and various structures of monolayer (ML) InSe, α-In_2Se_3 and β-In_2Se_3 are revealed by scanning transmission electron microscopy (STEM). A large negative magnetoresistance up to 40% at 2 K under 9 T out-of-plane magnetic field is consistently observed in the structures.

The experiments were performed on a homemade MBE system with a base pressure lower than 2×10^{-10} torr. The semi-insulating InP(111)B substrates were ultrasonically cleaned by acetic acid and acetone successively for 20 min each before being transferred into the MBE chamber. The substrates were degassed at 380℃ by indirect heating for 5 h and then annealed at 430℃ for 20 min to eliminate oxides and obtain clean and flat surfaces. High-purity Se was deposited from a standard Knudsen cell. Atomic Zr flux was supplied by a high-purity Zr rod of 2 mm diameter in an e-beam evaporator. Due to the low vapor pressure of Zr even at its melting point, this material was deposited at a low flux rate down to 0.01 ML/min with a heating power of 24 W. During growth, the temperature of substrates was fixed at 400℃, at which the deposited atoms react with indium in the substrate to form $ZrSe_2$ and In_xSe_y, respectively. The residue P atoms were then desorbed into vacuum. The MBE growth was monitored by *in situ* reflection high energy electron diffraction (RHEED).

The lattices of InP and $ZrSe_2$ can be clearly resolved by RHEED (Fig. 1(a)). The (111) oriented surface of the zincblende InP has an in-plane lattice constant of 4.15 Å.[46] Bulk $ZrSe_2$ is a CdI_2-type vdW material with lattice constants $a = b = 3.77$ Å and $c = 6.13$ Å.[47] However, the layered hexagonal InSe, α-In_2Se_3 and β-In_2Se_3 have similar in-plane lattice constants of ∼4.0 Å.[27–32] Thus, identifying different phases of In_xSe_y from RHEED patterns is difficult.

Two distinct growth modes exist depending on the flux ratio between Se and Zr. It is noted that no In_xSe_y emerges without the aid of Zr. If Se:Zr $< 15:1$, only the RHEED pattern of $ZrSe_2$ will appear. If Se:Zr $> 30:1$, $ZrSe_2$ will be briefly visible in the RHEED pattern at the beginning of growth. Then the RHEED pattern switches to that of In_xSe_y. Such behavior indicates the film structure as shown in Figs. 1(b) and 1(c). As the growth continues, both Zr and In atoms diffuse through the film,[48] but in the opposite directions. As a result, $ZrSe_2$ always forms adjacent to the substrate and In_xSe_y floats on top of $ZrSe_2$. It is suggested that the surface will be passivated by Se without the involvement of Zr. Zr atoms help to break the In–Se bonds, making it possible for the In atoms to persistently diffuse to the top. Given the substrate temperature and the Zr flux rate, the growth modes can be simply controlled by the Se flux rate during the growth. Figure 1(d) shows a typical morphology characterization of the second mode by atomic force microscopy (AFM), which indicates a layer-plus-island growth pattern of both modes.

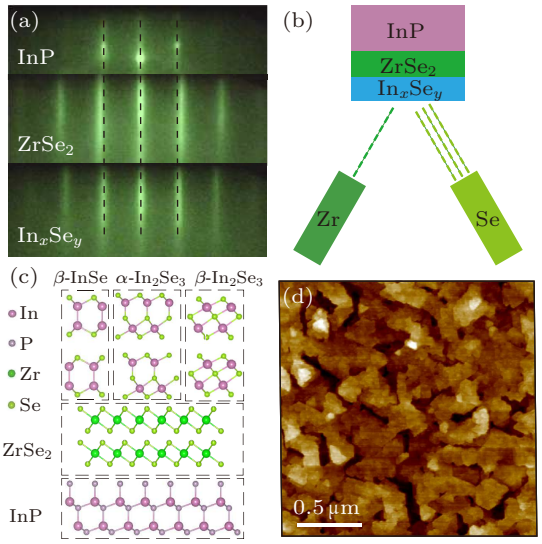

Fig. 1. (a) RHEED patterns of InP, $ZrSe_2$ and In_xSe_y in the epitaxial growth process. (b) An illustration of the MBE growth. (c) Lattice structures of InP, $ZrSe_2$, β-InSe, α-In_2Se_3 and β-In_2Se_3. (d) A typical morphology characterization of the sample with In_xSe_y top layers by AFM.

The In_xSe_y/$ZrSe_2$ structure is confirmed by STEM. Samples prepared with large Se:Zr ratio and capped with amorphous Se are investigated by STEM measurements. Figure 2 shows the typical atomically resolved high-angle annular dark-field (HAADF) images of the heterostructure viewed along the ⟨100⟩ direction. It demonstrates that 1 T-$ZrSe_2$ layers are sandwiched between the InP substrate and In_xSe_y layers. The $ZrSe_2$ layers are flat in a large scale with the same in-plane lattice constant as that of the bulk. However, the translational symmetry along the c-axis is broken and the out-of-plane lattice constant is enlarged to ∼6.30 Å, giving rise to even more two-dimensional characteristics. The In_xSe_y layers can be distinguished from $ZrSe_2$ by evidently larger in-plane lattice constants. Compared with the existing structure models, different archetypes can be identified in the polymorphic In_xSe_y, including InSe (Se–In–In–Se), α-In_2Se_3 and β-In_2Se_3 (Se–In–Se–In–Se). All of these species are able to interface with $ZrSe_2$. Inter-

estingly, if the flux ratio of Se and Zr is decreased after the emergence of In_xSe_y during growth, the $ZrSe_2$ layers will reappear on top of In_xSe_y as shown in Fig. 2(c).

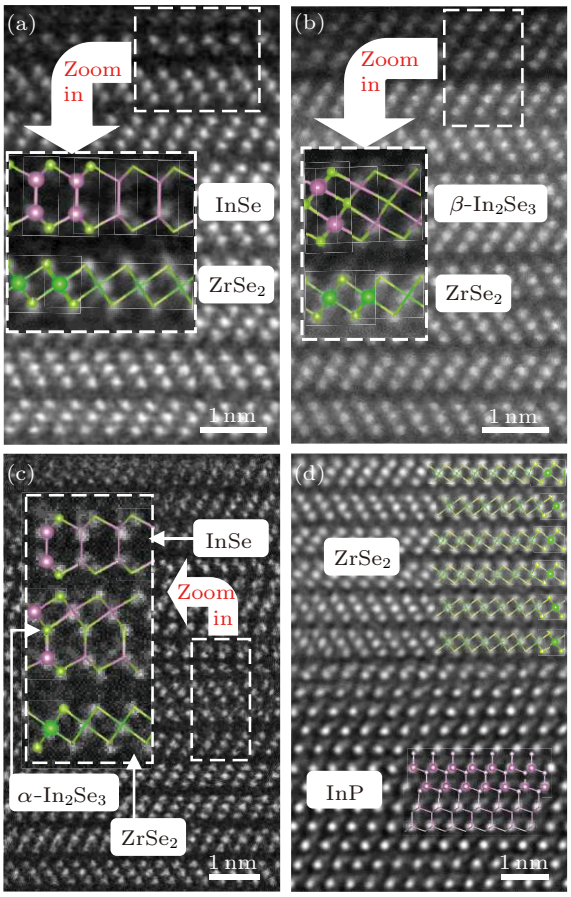

Fig. 2. HAADF-STEM images of $In_xSe_y/ZrSe_2/InP(111)$ heterostructures viewed along the ⟨100⟩ direction. (a) InSe at the interface of $In_xSe_y/ZrSe_2$. (b) β-In_2Se_3 at the interface of $In_xSe_y/ZrSe_2$. (c) In_xSe_y sandwiched by $ZrSe_2$. (d) The interface between the $ZrSe_2$ layer and the InP substrate.

Figure 3(a) exhibits the atomic-resolved scanning tunneling microscopy (STM) image of the $ZrSe_2$ layer. The hexagonal lattice structure and the in-plane lattice constant of 3.8 Å are consistent with the STEM and RHEED results. The scanning tunneling spectroscopy (STS) measurement on $ZrSe_2$ (Fig. 3(b)) shows a bandgap of 1.1 eV, which is larger than that of bulk $ZrSe_2$ (∼0.9 eV) and close to that of monolayer $ZrSe_2$ (∼1.2 eV) determined by angle resolved photoemission spectroscopy (ARPES).[49] The surface of In_xSe_y (Fig. 3(c)) has a $\sqrt{3}\times\sqrt{3}$ reconstruction with the lattice constant of 6.93 Å ($\sqrt{3}\times 4.0$ Å). The energy bandgap (Fig. 3(d)) is 1.4 eV, located between the levels of the bulk and the monolayer InSe.[21]

The insulator behavior of $ZrSe_2$ layers is confirmed by *ex situ* transport measurement using van der Pauw geometry.[50] The resistivity of the $ZrSe_2$ sample prepared with a flux ratio of Se:Zr ∼15:1 is too large to be measured even at room temperature. The film can become more conducting by reducing the flux ratio Se:Zr to be less than 5:1 in order to generate enough Se vacancies. A positive magnetoresistance of ∼10% under 9 T is found at 2 K in these heavily doped $ZrSe_2$ films as shown in Fig. 4(a).

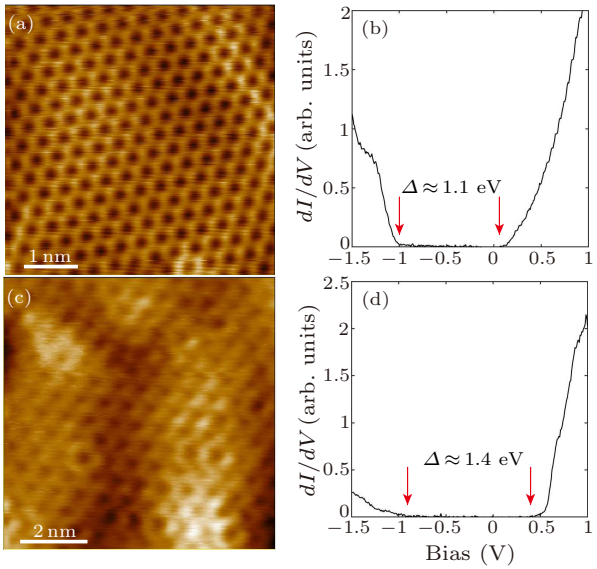

Fig. 3. (a) and (b) Atomic-resolved STM image of a 10-layer $ZrSe_2$ and STS. (c) and (d) Atomic-resolved STM image of In_xSe_y monolayer and STS.

The $In_xSe_y/ZrSe_2$ heterostructure behaves as a semiconductor (Fig. 4(b)). The sign of Hall resistance (Fig. 4(c)) reveals that the carriers in the samples are of n-type, indicating Se vacancies as the main doping source. The R_{xy}–B curve (Fig. 4(c)) shows good linearity in the range of 0–9 T below 200 K. The sheet carrier density (Fig. 4(d)) calculated from the Hall resistance increases gradually with decreasing temperature, peaked at 90 K (∼1.2×10^{13} cm^{-2}), and decreases quickly to the minimum at 2 K (∼5.2×10^{12} cm^{-2}). On the other hand, the Hall mobility (Fig. 4(e)) drops monotonically with decreasing temperature. The mobility at room temperature (∼160 $cm^2\cdot V^{-1}s^{-1}$) is larger than that of the In_xSe_y epitaxially grown on other lattice-mismatching substrates,[41,42] but still not comparable with the record of 1055 $cm^2\cdot V^{-1}s^{-1}$ by using exfoliated samples.[17]

Figure 4(f) is the typical magnetoresistance for the $In_xSe_y/ZrSe_2$ heterostructure. Under an out-of-plane magnetic field up to 9 T, all the films show similar negative magnetoresistance effect at low temperature with no hysteresis. At 2 K, the sheet resistivity decreases rapidly with increasing field and tends to saturate at ∼40% level under 9 T regardless of the different zero-field resistivity and film thickness of $ZrSe_2$ underneath. The negative magnetoresistance effect becomes weaker when the temperature arises, but can still be visible at 150 K. The observed negative magnetoresistance cannot be explained by the weak localiza-

tion theory[51] since the conductivity (∼1 μS) at 2 K of most samples is much less than the conductance quantum ($e^2/h \sim 39\,\mu$S). It could be related to other effects, such as electron-electron or electron-phonon interactions. Among the three species of In_xSe_y, we are still not able to identify which one contributes to the observed negative magnetoresistance. Both InSe and In_2Se_3 have been reported to show negative magnetoresistance[52,53] and we expect them to play roles in the current case.

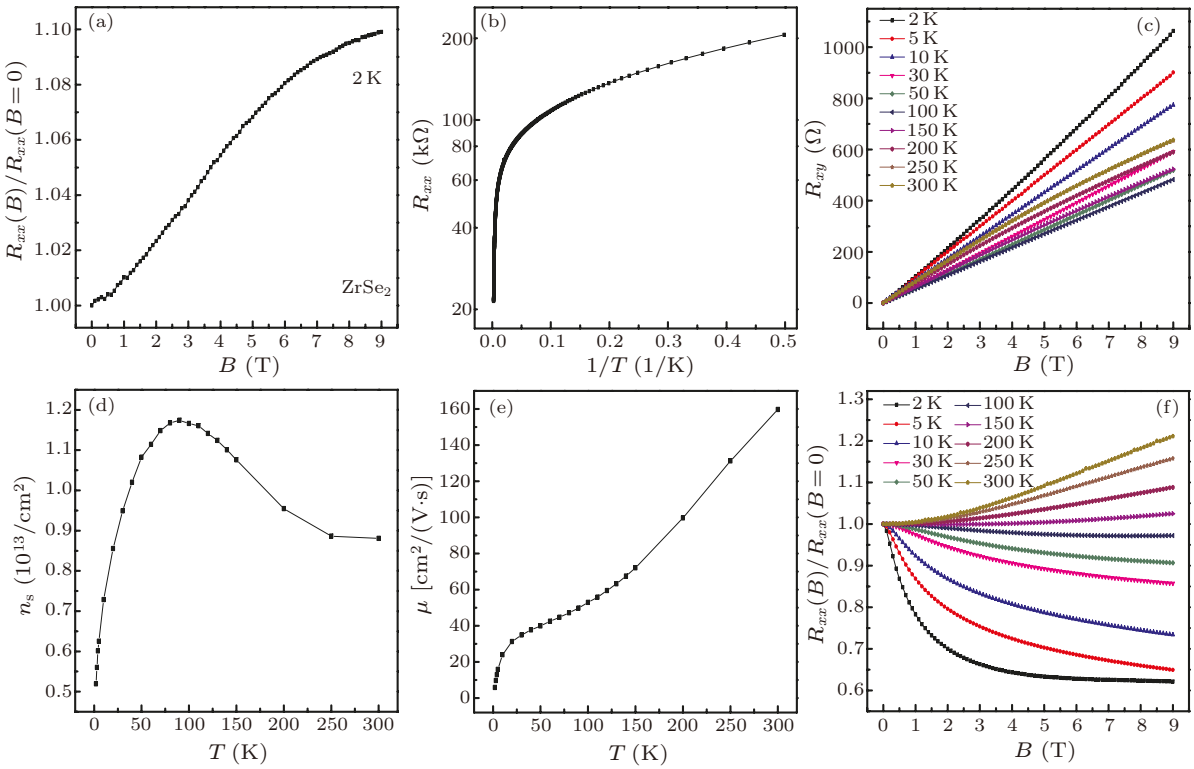

Fig. 4. (a) Typical positive magnetoresistance of the heavily doped $ZrSe_2$ layers grown on the InP(111) substrate at 2 K. (b)–(e) Transport measurement of a sample consisting of two layers of InSe and two layers of In_2Se_3 sandwiched between 12 layers of $ZrSe_2$ at the bottom and 4 layers of $ZrSe_2$ on the top. The magnetic field dependence of the Hall resistance R_{xy} shows good linearity under 200 K. The sheet carrier density n_s peaks at 90 K when $n_s = 1.2 \times 10^{13}\,\mathrm{cm}^{-2}$. The Hall mobility μ is $160\,\mathrm{cm}^2\cdot\mathrm{V}^{-1}\mathrm{s}^{-1}$ at 300 K, and decrease monotonically while cooling down to 2 K. (f) Typical magnetoresistance of $In_xSe_y/ZrSe_2$/InP(111) heterostructure at various temperatures ranging from 2 K to 300 K.

In conclusion, by co-depositing Zr and Se onto InP(111) substrates, we have successfully grown the polymorphic In_xSe_y layers on top of the insulating $ZrSe_2$. It is found that selenium flux together with the indium atoms from InP substrates are not enough to grow In_xSe_y. Zirconium is needed to avoid surface passivation and help to form layers of In_xSe_y persistently. The establishment of this MBE growth recipe of $In_xSe_y/ZrSe_2$ heterostructure with good lattice matching creates new opportunity to fabricate indium selenide devices.

We thank Ding Zhang for valuable discussion.

References

[1] Fiori G, Bonaccorso F, Iannaccone G *et al.* 2014 *Nat. Nanotechnol.* **9** 768
[2] Marks T J and Hersam M C 2015 *Nature* **520** 631
[3] Franklin A D 2015 *Science* **349** aab2750
[4] Butler S Z, Hollen S M, Cao L *et al.* 2013 *ACS Nano* **7** 2898
[5] Zhao M, Ye Y, Han Y *et al.* 2016 *Nat. Nanotechnol.* **11** 954
[6] Novoselov K S, Geim A K, Morozov S V *et al.* 2004 *Science* **306** 666
[7] Li L, Yu Y, Ye G J *et al.* 2014 *Nat. Nanotechnol.* **9** 372
[8] Wang Q H, Kalantar-Zadeh K, Kis A *et al.* 2012 *Nat. Nanotechnol.* **7** 699
[9] Chhowalla M, Shin H S, Eda G *et al.* 2013 *Nat. Chem.* **5** 263
[10] Splendiani A, Sun L, Zhang Y *et al.* 2010 *Nano Lett.* **10** 1271
[11] Radisavljevic B, Radenovic A, Brivio J *et al.* 2011 *Nat. Nanotechnol.* **6** 147
[12] Li M Y, Shi Y, Cheng C C *et al.* 2015 *Science* **349** 524
[13] Hu P, Wen Z, Wang L *et al.* 2012 *ACS Nano* **6** 5988
[14] Late D J, Liu B T, Luo J *et al.* 2012 *Adv. Mater.* **24** 3549
[15] Lei S, Ge L, Liu Z *et al.* 2013 *Nano Lett.* **13** 2777
[16] Huang W, Gan L, Li H *et al.* 2016 *CrystEngComm* **18** 3968
[17] Feng W, Zheng W, Cao W *et al.* 2014 *Adv. Mater.* **26** 6587
[18] Tamalampudi S R, Lu Y, Kumar U R *et al.* 2014 *Nano Lett.* **14** 2800
[19] Jacobsgedrim R B, Shanmugam M, Jain N *et al.* 2014 *ACS Nano* **8** 514

[20] Bandurin D A, Tyurnina A V, Yu G *et al.* 2017 *Nat. Nanotechnol.* **12** 223
[21] Mudd G W, Svatek S A, Ren T *et al.* 2013 *Adv. Mater.* **25** 5714
[22] Choi M S, Cheong B, Ra C H *et al.* 2017 *Adv. Mater.* **29** 1703568
[23] Cui C, Hu W, Yan X *et al.* 2018 *Nano Lett.* **18** 1253
[24] Poh S M, Tan S J, Wang H *et al.* 2018 *Nano Lett.* **18** 6340
[25] Kibirev I A, Matetskiy A V, Zotov A V *et al.* 2018 *Appl. Phys. Lett.* **112** 191602
[26] Si M W, Saha A K, Gao S J *et al.* 2019 *Nat. Electron.* **2** 580
[27] Popović S, Tonejc A, Gržeta-Plenković B *et al.* 1979 *J. Appl. Crystallogr.* **12** 416
[28] Manolikas C 1988 *J. Solid State Chem.* **74** 319
[29] Osamura K, Murakami Y and Tomile Y 1966 *J. Phys. Soc. Jpn.* **21** 1848
[30] Miyazawa H and Sugaike S 1957 *J. Phys. Soc. Jpn.* **12** 312
[31] Čelustka B and Bidjin D 1971 *Phys. Status Solidi A* **6** 301
[32] Kupers M, Konze P M, Meledin A *et al.* 2018 *Inorg. Chem.* **57** 11775
[33] De Blasi C, Micocci G, Mongelli S *et al.* 1982 *J. Cryst. Growth* **57** 482
[34] Lin M, Wu D, Zhou Y *et al.* 2013 *J. Am. Chem. Soc.* **135** 13274
[35] Ohtsuka T, Nakanishi K, Okamoto T *et al.* 2001 *Jpn. J. Appl. Phys.* **40** 509
[36] Emery J Y, Brahimostmane L, Hirlimann C *et al.* 1992 *J. Appl. Phys.* **71** 3256
[37] Hayashi T, Ueno K, Saiki K *et al.* 2000 *J. Cryst. Growth* **219** 115
[38] Sanchez-Royo J F, Segura A, Lang O *et al.* 2001 *J. Appl. Phys.* **90** 2818
[39] Balakrishnan N, Steer E D, Smith E F *et al.* 2018 *2D Mater.* **5** 035026
[40] Amokrane A, Proix F, Monkad S E *et al.* 1999 *J. Phys.: Condens. Matter* **11** 4303
[41] Zhou J D, Zeng Q S, Lv D H *et al.* 2015 *Nano Lett.* **15** 6400
[42] Yang Z B, Jie W J, Mak C H *et al.* 2017 *ACS Nano* **11** 4225
[43] Zheng W, Xie T, Zhou Y *et al.* 2015 *Nat. Commun.* **6** 6972
[44] Zhou S, Tao X, Gu Y *et al.* 2016 *J. Phys. Chem. C* **120** 4753
[45] Okamoto T, Nakada Y, Aoki T *et al.* 2006 *Phys. Status Solidi C* **3** 2796
[46] Massidda S, Continenza A, Freeman A J *et al.* 1990 *Phys. Rev. B* **41** 12079
[47] Whitehouse C R and Balchin A A 1978 *Phys. Status Solidi A* **47** K173
[48] Balluffi R W and Bkakely J M 1975 *Thin Solid Films* **25** 363
[49] Mleczko M J, Zhang C, Lee H R *et al.* 2017 *Sci. Adv.* **3** e1700481
[50] Pauw L J 1958 *Philips Res. Rep.* **13** 1
[51] Hikami S, Larkin A I and Nagaoka Y 1980 *Prog. Theor. Phys.* **63** 707
[52] Dmitriev A I, Kovalyuk Z D, Lazorenko V I *et al.* 1990 *Phys. Status Solidi B* **162** 213
[53] Romeo N 1974 *Phys. Status Solidi A* **26** K187